Modelling of primary alkaline battery cathodes: A simplified model

J.F. Johansen [a,*], T.W. Farrell [a], C.P. Please [b]

[a] *School of Mathematical Sciences, Queensland University of Technology, GPO Box 2434, Brisbane, Qld. 4001, Australia*
[b] *School of Mathematics, University of Southampton, Southampton SO17 1BJ, UK*

Abstract

A simplified model, to that produced previously by the authors, for the galvanostatic discharge of primary alkaline battery cathodes is presented. Laplace transform and perturbation methods are employed to obtain the leading order spatial and temporal behaviour of the porous cathode over two distinct size scales. It is shown that for a wide range of industrially relevant discharge conditions the time taken for KOH electrolyte to diffuse into a porous electrolytic manganese dioxide particle is fast compared with the cathodic discharge time and that ohmic losses within the graphite phase of the cathode can be considered to be negligible. Numerical solution of the simplified model equations is discussed and the results are validated against relevant experimental data.
© 2005 Elsevier B.V. All rights reserved.

Keywords: Primary alkaline battery; Cathode; Electrolytic manganese dioxide; Mathematical model; Perturbation methods

1. Introduction

Primary alkaline battery cathodes are compacted mixtures of fine particles of electrolytic manganese dioxide (EMD) and graphite that are flooded with concentrated (7–10 M) aqueous potassium hydroxide (KOH). Cathodes are usually constructed with relative weight percentages of approximately 80–87% EMD, 5–12% graphite and 6–12% KOH [1]. These cathodes are complex porous structures, and their discharge behaviour is the result of interconnected and non-linear physical, chemical and electrochemical phenomena that occur over several size scales. Development of improved battery materials and systems requires a sound understanding of these processes.

Mathematical modelling provides a unique opportunity to understand the processes and their interactions that determine the discharge behaviour of primary alkaline battery cathodes. Such modelling can also provide direction for further research and explanations for experimental observations.

In a series of papers, Newman and co-workers [2–8] developed an approach to modelling porous electrodes, referred to as Macrohomogeneous Porous Electrode Theory. This approach has been used as a basis for a number of alkaline battery models, including those of Wruck [9], Chen and Cheh [10,11], Podlaha and Cheh [12,13], Zhang and Cheh [14], Farrell et al. [15], and Kriegsmann and Cheh [16].

To date, the systematic analysis of previous models has been largely restricted to sensitivity arguments that involve a small sub-set of parameters within the model system in question. A more general sensitivity analysis, however, has been undertaken by Zhang and Cheh [17] for the alkaline battery model originally posed by Chen and Cheh [10]. Furthermore, Farrell and Please [1] applied perturbation methods in order to analyse a set of equations, previously developed by Farrell et al. [15], for the galvanostatic discharge of a single porous particle of EMD. Their work led to significant simplifications and a greater knowledge of the behaviour of particle discharge. Nevertheless, we note that no experimental validation of their results was presented because individual particle discharge at the size scales found within commercial cathodes is difficult.

Nomenclature

a	activity of a dissolved species (mol cm^{-3})
A, B	arbitrary constants
C	concentration (mol cm^{-3})
$\bar{C}_{Mn^{4+}}$	Laplace transform of $C_{Mn^{4+}}$
$\hat{C}_{e,0,1,\ldots}$	terms of the asymptotic expansion of $\hat{C}_e$ in α_5
$D_{e\infty}$	diffusion coefficient of KOH (cm^2 s^{-1})
f	function used to solve auxiliary Eq. (40).
F	Faraday's constant (C mol^{-1})
H	height of cathode (cm)
i	current density (A cm^{-2})
i_n	transfer current density from oxide to solution phase (A cm^{-2})
i_0^0	initial equilibrium exchange current density (A cm^{-2})
I	total discharge current (A)
k_2, k_3	constants associated with calculating the conductivity of EMD
L	the Laplace transform function
p	Laplace transform variable
r	radial coordinate on the particle scale (cm)
r_o	outer radius of particle (cm)
R	radial coordinate on the cathode scale (cm)
R_{gas}	universal gas constant (J K^{-1} mol^{-1})
R_i	inner radius of cathode (cm)
R_o	outer radius of cathode (cm)
t	time (s)
t^*	dummy variable used in integrals
t_{K^+}	transport (transference) number for K$^+$
T	temperature (K)
$v^{\square}$	volume-average velocity of electrolyte (cm s^{-1})
$\bar{V}_e$	partial molar volume of electrolyte (cm^3 mol^{-1})
$\bar{V}_{H_2O}$	partial molar volume of H$_2$O (cm^3 mol^{-1})
$\bar{V}_{Mn^{3+}}$	partial molar volume of Mn^{3+} (cm^3 mol^{-1})
$\bar{V}_{Mn^{4+}}$	partial molar volume of Mn^{4+} (cm^3 mol^{-1})
y	radial coordinate on the crystal scale (cm)
y_o	outer radius of EMD crystal (cm)

Greek

α_{1-17}	dimensionless constants associated with the dimensionless equation set
ε_{EMD}	fraction of total cathode volume that is EMD
ε_s	fraction of the cathode volume that is void
η	local overpotential (V)
$\kappa_{e\infty}$	conductivity of bulk electrolyte solution (S cm^{-1})
λ_n	the positive roots of Eq. (28)
σ_g	conductivity of bulk graphite (S cm^{-1})

Superscripts

0	value at $t = 0$ s

Subscripts

e	electrolyte phase
Mn^{4+}	manganese 4+ ion
p	manganese oxide particle scale

In this work, we begin by considering the full cathodic discharge model proposed by Farrell et al. [15], which was shown to compare favourably with available galvanostatic discharge data. Our aim is to apply perturbation methods in order to analyse the key physical, chemical and electrochemical processes that govern the behaviour of the model and, in so doing, obtain a simplified model system that accounts for these key processes. This work extends the work of Farrell and Please [1] into the cathodic domain and yields a simplified model with solutions that can be directly validated against experimental data. Such validation is presented here.

2. Model development

2.1. Full cathode model

To model effectively the processes that occur in the multi-scale environment of an alkaline battery cathode, Farrell et al. [15] employ a simplified description of the cathode. In their model, the EMD and graphite in the cathode are assumed to be well mixed, that is, each porous EMD particle is surrounded by a continuous graphite phase that connects the porous EMD particles to the current-collector. These porous EMD particles consist of aggregates of non-porous EMD crystals. Both crystals and particles are assumed to be spherical. In addition, the network of pores within the EMD particles and between the EMD and graphite particles is assumed to be flooded with concentrated aqueous KOH electrolyte solution. A schematic diagram of these size scales is given in Fig. 1. Furthermore, the Mn^{4+} ions within the crystals are assumed to only undergo the first electron reduction step as given by the reaction,

$$MnO_2 + H_2O + e^- \Leftrightarrow MnOOH + OH^- \tag{1}$$

The governing equations and associated boundary and initial conditions previously introduced by Farrell et al. [15] to describe the galvanostatic discharge of the three-scale structure depicted in Fig. 1 are summarised below. The equations are given in dimensionless form below.

The crystal scale:

$$\alpha_1 \frac{\partial \hat{C}_{Mn^{4+}}}{\partial \hat{t}} = \frac{1}{\hat{y}^2} \frac{\partial}{\partial \hat{y}} \left(\hat{y}^2 \frac{\partial \hat{C}_{Mn^{4+}}}{\partial \hat{y}} \right), \tag{2}$$
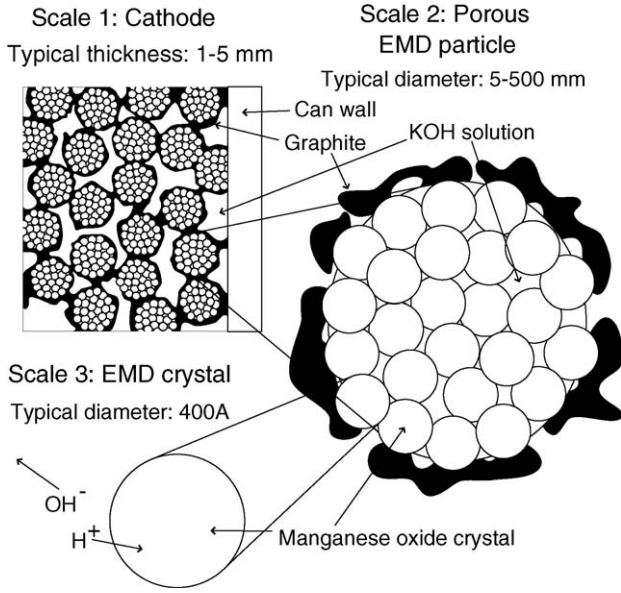
Fig. 1. Schematic diagram of three size scales within a primary alkaline battery cathode.

$$\left.\frac{\partial \hat{C}_{Mn^{4+}}}{\partial \hat{y}}\right|_{\hat{y}=0} = 0, \tag{3}$$

$$\left.\frac{\partial \hat{C}_{Mn^{4+}}}{\partial \hat{y}}\right|_{\hat{y}=1} = \alpha_1 \hat{i}_n, \tag{4}$$

$$\hat{i}_n = \alpha_2 \left\{ \left(\frac{1 - \alpha_3 \hat{C}_{Mn^{4+}}|_{\hat{y}=1}}{1 - \alpha_3} \right) \hat{C}_{e(p)} \exp\left(\alpha_{14} \hat{\eta}_{(p)} + \alpha_{15} \left(1 - \hat{C}_{Mn^{4+}}|_{\hat{y}=1} \right) \right) \right.$$
$$\left. - \hat{C}_{Mn^{4+}}|_{\hat{y}=1} \left(\frac{1 - \alpha_4 \hat{C}_{e(p)}}{1 - \alpha_4} \right) \exp\left(-\alpha_{14} \hat{\eta}_{(p)} - \alpha_{15} \left(1 - \hat{C}_{Mn^{4+}}|_{\hat{y}=1} \right) \right) \right\}, \tag{5}$$

$$\hat{C}_{Mn^{4+}}|_{\hat{t}=0} = 1. \tag{6}$$

The particle scale:

$$\frac{1}{\hat{r}^2} \frac{\partial}{\partial \hat{r}} (\hat{r}^2 \hat{i}_{e(p)}) = 3\hat{i}_n, \tag{7}$$

$$\frac{1}{\hat{r}^2} \frac{\partial}{\partial \hat{r}} (\hat{r}^2 \hat{v}_{(p)}^{\square}) = 3\hat{i}_n, \tag{8}$$

$$\alpha_5 \frac{\partial \hat{C}_{e(p)}}{\partial \hat{t}} = \frac{1}{\hat{r}^2} \frac{\partial}{\partial \hat{r}} \left(\hat{D}_{e\infty} \hat{r}^2 \frac{\partial \hat{C}_{e(p)}}{\partial \hat{r}} \right) - 3\alpha_5 \alpha_6 \hat{i}_n$$
$$- \frac{\alpha_5 \alpha_7}{\hat{r}^2} \frac{\partial}{\partial \hat{r}} (\hat{r}^2 \hat{C}_{e(p)} \hat{v}_{(p)}^{\square}), \tag{9}$$

$$\frac{\partial \hat{\eta}_{(p)}}{\partial \hat{r}} = \hat{i}_{e(p)} \left[\frac{1}{\left(\hat{C}_{Mn^{4+}}|_{\hat{y}=0.8} \right)^{k_3}} + \frac{\alpha_8}{\hat{\kappa}_{e\infty}} \right]$$
$$+ \alpha_9 \left[1 + \frac{\alpha_{10} \hat{C}_{e(p)}}{1 - \alpha_4 \hat{C}_{e(p)}} \right] \frac{\partial \ln \hat{a}_{e(p)}}{\partial \hat{C}_{e(p)}} \frac{\partial \hat{C}_{e(p)}}{\partial \hat{r}}, \tag{10}$$

$$\hat{C}_{e(p)}|_{\hat{r}=1} = \hat{C}_e, \tag{11}$$

$$\hat{\eta}_{(p)}|_{\hat{r}=1} = \hat{\eta}, \tag{12}$$

$$\left.\frac{\partial \hat{C}_{e(p)}}{\partial \hat{r}}\right|_{\hat{r}=0} = 0, \tag{13}$$

$$\hat{v}_{(p)}^{\square}\Big|_{\hat{r}=0} = 0, \tag{14}$$

$$\left.\frac{\partial \hat{\eta}_{(p)}}{\partial \hat{r}}\right|_{\hat{r}=0} = 0, \tag{15}$$

$$\hat{C}_{e(p)}|_{\hat{t}=0} = 1. \tag{16}$$

The cathode scale:

$$\frac{1}{\alpha_{17} + \hat{R}} \frac{\partial}{\partial \hat{R}} ((\alpha_{17} + \hat{R})\hat{i}_e) = 3\hat{i}_{e(p)}|_{\hat{r}=1}, \tag{17}$$

$$\frac{1}{\alpha_{17} + \hat{R}} \frac{\partial}{\partial \hat{R}} \left((\alpha_{17} + \hat{R}) \hat{v}^{\square} \right) = 3\hat{v}_{(p)}^{\square}\Big|_{\hat{r}=1}, \tag{18}$$

$$\frac{\alpha_5}{\alpha_{16}^2} \sqrt{\frac{\varepsilon_{s(p)}}{\varepsilon_s}} \frac{\partial \hat{C}_e}{\partial \hat{t}} = \frac{1}{\alpha_{17} + \hat{R}} \frac{\partial}{\partial \hat{R}} \left(\hat{D}_{e\infty} (\alpha_{17} + \hat{R}) \frac{\partial \hat{C}_e}{\partial \hat{R}} \right)$$
$$- \frac{\alpha_5 \alpha_7 \alpha_{11}}{\alpha_{16}^2} \frac{1}{\alpha_{17} + \hat{R}} \frac{\partial}{\partial \hat{R}} ((\alpha_{17} + \hat{R})\hat{v}^{\square}\hat{C}_e)$$
$$- \frac{3\alpha_{11}}{\alpha_{16}^2} \left(\hat{D}_{e\infty} \frac{\partial \hat{C}_{e(p)}}{\partial \hat{r}} - \alpha_5 \alpha_7 \hat{v}_{(p)}^{\square} \hat{C}_{e(p)} \right)\Big|_{\hat{r}=1}, \tag{19}$$

$$\frac{\partial \hat{\eta}}{\partial \hat{R}} = \frac{\alpha_{12}}{\alpha_{16}^2} \hat{i}_e \left(\frac{1}{\hat{\kappa}_{e\infty}} + \alpha_{13} \right) - \frac{\alpha_{12}\alpha_{13}\alpha_{17}}{\alpha_{16}^2 (\alpha_{17} + \hat{R})}$$
$$+ \alpha_9 \left[1 + \frac{\alpha_{10} \hat{C}_e}{1 - \alpha_4 \hat{C}_e} \right] \frac{\partial \ln \hat{a}_e}{\partial \hat{C}_e} \frac{\partial \hat{C}_e}{\partial \hat{R}}, \tag{20}$$

$$\hat{C}_e|_{\hat{R}=0} = 1, \tag{21}$$

$$\hat{i}_e|_{\hat{R}=0} = 1, \tag{22}$$

$$\hat{i}_e|_{\hat{R}=1} = 0, \tag{23}$$

$$\hat{v}^{\square}\Big|_{\hat{R}=1} = 0, \tag{24}$$

$$\left.\frac{\partial \hat{C}_e}{\partial \hat{R}}\right|_{\hat{R}=1} = 0, \tag{25}$$

$$\hat{C}_e|_{\hat{t}=0} = 1. \tag{26}$$

Hereafter, we refer to Eqs. (2)–(26) as the *full cathode model*.

Table 1
Dimensionless variables

$$\hat{y} = \frac{y}{y_o}$$

$$\hat{r} = \frac{r}{r_o}$$

$$\hat{R} = \frac{R - R_i}{R_o - R_i}$$

$$\hat{C}_{Mn^{4+}} = \frac{C_{Mn^{4+}}}{C_{Mn^{4+}}^0}$$

$$\hat{C}_{e(p)} = \frac{C_{e(p)}}{C_e^0}$$

$$\hat{C}_e = \frac{C_e}{C_e^0}$$

$$\hat{i}_e = \frac{2\pi R_i H}{I} i_e$$

$$\hat{D}_{e\infty} = \frac{D_{e\infty}}{D_{e\infty}^0}$$

$$\hat{i}_n = \frac{2\pi R_i H (R_o - R_i) \varepsilon_{EMD}}{I y_o} i_n$$

$$\hat{v}_{(p)}^\square = \frac{2\pi R_i H (R_o - R_i) \varepsilon_{EMD} F}{r_o \left(\bar{V}_{H_2O} - t_{K^+}^\square \bar{V}_e\right) I \left(1 - \varepsilon_{s(p)}\right)} v_{(p)}^\square$$

$$\hat{v}^\square = \frac{2\pi R_i H F}{\left(\bar{V}_{H_2O} - t_{K^+}^\square \bar{V}_e\right) I} v^\square$$

$$\hat{\eta}_{(p)} = \frac{2\pi R_i H (R_o - R_i) \varepsilon_{EMD} k_2}{r_o^2 I} \eta_{(p)}$$

$$\hat{\eta} = \frac{2\pi R_i H (R_o - R_i) \varepsilon_{EMD} k_2}{r_o^2 I} \eta$$

$$\hat{t} = \frac{I}{2\pi R_i H (R_o - R_i) \varepsilon_{EMD} F C_{Mn^{4+}}^0} t$$

$$\hat{i}_{e(p)} = \frac{2\pi R_i H (R_o - R_i) \varepsilon_{EMD}}{I \left(1 - \varepsilon_{s(p)}\right) r_o} i_{e(p)}$$

$$\hat{\kappa}_{e\infty} = \frac{\kappa_{e\infty}}{\kappa_{e\infty}^0}$$

The relationships between dimensionless variables in the above equations and their dimensioned counterparts are listed in Table 1.

The dimensionless constants α_1–α_{17} appearing in Eqs. (2)–(26) are listed in Table 2 along with their typical value ranges. In obtaining the typical ranges for these parameters, the discharge rate has been varied from 5 to 200 mA g^{-1} of EMD, the particle radius (r_o) from 5 to 250 μm, and the cathode thickness ($R_o - R_i$) from 0.5 to 5 mm. Such variations are indicative of the industrially relevant ranges of these parameters [18]. The remaining parameter values used to calculate the typical ranges given in Table 2 are given in Tables 3 and 4. The dimensionless constants used here are similar to those used by Farrell and Please [1] for their particle scale model, but here the constants relate to the time scale of cathodic discharge rather than the time scale of particle discharge.

3. Simplified cathode model

We now systematically reduce the full system of model equations introduced above in order to obtain a simplified model that retains the essential physical, chemical and electrochemical phenomena that comprise the discharge of a primary alkaline battery cathode.

The initial boundary value problem given by Eqs. (2)–(4) and (6) is simplified by applying the method of Laplace transforms (See for example, Trim [19]) to obtain a single expression, which governs the concentration distribution of Mn^{4+} within an EMD crystal. Details are given in Appendix A, where we show that:

$$\hat{C}_4 \left(\hat{y}, \hat{t}\right) = 1 + 3 \int_0^{\hat{t}} \hat{i}_n \, dt^* + \frac{2}{\hat{y}} \sum_{m=1}^{\infty} \frac{\sin (\lambda_m \hat{y})}{\sin (\lambda_m)}$$

$$\times \int_0^{\hat{t}} \hat{i}_n \big|_{\hat{t} = \hat{t} - t^*} \exp \left(\frac{-\lambda_m^2 t^*}{\alpha_1}\right) dt^*, \qquad (27)$$

Table 2
Dimensionless constants and their typical range of values

Dimensionless constant	Typical range
$\alpha_1 = \dfrac{I y_o^2}{2\pi R_i H (R_o - R_i) \varepsilon_{EMD} D_{H^+} C_{Mn^{4+}}^0 F}$	$0.032 \leq \alpha_1 \leq 1.3$
$\alpha_2 = \dfrac{2\pi R_i H (R_o - R_i) \varepsilon_{EMD} i_0^0}{I y_o}$	$0.022 \leq \alpha_2 \leq 0.87$
$\alpha_3 = \bar{V}_{Mn^{3+}} C_{Mn^{4+}}^0$	1
$\alpha_4 = \bar{V}_e C_e^0$	0.16
$\alpha_5 = \dfrac{r_o^2 I}{2\pi R_i H (R_o - R_i) \varepsilon_{EMD} D_{e\infty}^0 \sqrt{\varepsilon_{s(p)}} F C_{Mn^{4+}}^0}$	$5.5 \times 10^{-9} \leq \alpha_5 \leq 0.014$
$\alpha_6 = \dfrac{t_{K^+}^\square C_{Mn^{4+}}^0}{\varepsilon_{s(p)} C_e^0}$	12
$\alpha_7 = \dfrac{\left(\bar{V}_{H_2O} - t_{K^+}^\square \bar{V}_e\right) \left(1 - \varepsilon_{s(p)}\right) C_{Mn^{4+}}^0}{\varepsilon_{s(p)}}$	6.4
$\alpha_8 = \dfrac{k_2 \left(1 - \varepsilon_{s(p)}\right)}{\kappa_{e\infty}^0 \sqrt{\varepsilon_{s(p)}^3}}$	9.7×10^4
$\alpha_9 = \dfrac{4\pi R_i H (R_o - R_i) \varepsilon_{EMD} R_{gas} T t_{K^+}^\square k_2}{F r_o^2 I}$	$3000 \leq \alpha_9 \leq 7.6 \times 10^9$
$\alpha_{10} = \dfrac{C_e^0 \bar{V}_{H_2O}}{t_{K^+}^\square}$	0.74
$\alpha_{11} = \dfrac{\varepsilon_{EMD} \sqrt{\varepsilon_{s(p)}^3}}{\left(1 - \varepsilon_{s(p)}\right) \sqrt{\varepsilon_s^3}}$	0.029
$\alpha_{12} = \dfrac{k_2 \varepsilon_{EMD}}{\kappa_{e\infty}^0 \sqrt{\varepsilon_s^3}}$	2800
$\alpha_{13} = \dfrac{\kappa_{e\infty}^0 \sqrt{\varepsilon_s^3}}{\sigma_g}$	8.3×10^{-10}
$\alpha_{14} = \dfrac{F r_o^2 I}{4\pi R_i H (R_o - R_i) \varepsilon_{EMD} R_{gas} T k_2}$	$2.9 \times 10^{-11} \leq \alpha_{14} \leq 7.2 \times 10^{-5}$
$\alpha_{15} = \dfrac{k_1 \bar{V}_{Mn^{3+}} C_{Mn^{4+}}^0 F}{2 R_{gas} T}$	6.8
$\alpha_{16} = \dfrac{r_o}{R_o - R_i}$	$2.0 \times 10^{-4} \leq \alpha_{16} \leq 0.5$
$\alpha_{17} = \dfrac{R_i}{R_o - R_i}$	$2000 \leq \alpha_{17} \leq 2.0 \times 10^4$

Table 3
Parameter values used in model

Parameter	Values and reference
C_e^0 (mol cm^{-3})	0.009 [22]
$C_{Mn^{4+}}$ (mol cm^{-3})	0.0486 [15]
D_{H^+} (cm^2 s^{-1})	1×10^{-15} [30]
F (C mol^{-1})	96485.309 [31]
i_0^0 (A cm^{-2})	5×10^{-8} [15]
k_1 (V)	0.35
k_2 (S cm^{-1})	1.5×10^2
k_3	4.328
R_{gas} (J K^{-1} mol^{-1})	8.31451 [31]
T (K)	298.15
t_{K^+}	0.22 [32]
$\bar{V}_e$ (cm^3 mol^{-1})	17.8 [33]
$\bar{V}_{H_2O}$ (cm^3 mol^{-1})	18.07 [33]
$\bar{V}_{Mn^{3+}}$ (cm^3 mol^{-1})	20.576
$\bar{V}_{Mn^{4+}}$ (cm^3 mol^{-1})	20.576
y_o (cm)	2.6×10^{-6} [22]
$\varepsilon_{EMD(p)}$	0.9 [22]
σ_g (S cm^{-1})	7×10^6 [31]

Table 4
Model input data for simulation of experimental set-up used by Williams [22]

Parameter	Value
Discharge rate (mA g^{-1} of EMD)	50
Particle radius, r_o (cm)	10×10^{-4}, 45×10^{-4}, 100×10^{-4} and 180×10^{-4}
Inner radius, R_i (cm)	1000.0
Outer radius, R_o (cm)	1000.5
Height, H (cm)	6.603×10^{-4}
Total mass of cathode (g)	4.5
Mass of EMD in cathode (g)	1.0
Mass of graphite in cathode (g)	2.9

where t^* is a dummy variable and the values of λ_m ($m = 1, 2, \ldots, \infty$) are given by the positive roots of

$$\tan(\lambda_m) - \lambda_m = 0. \tag{28}$$

Expression (27) replaces Eqs. (2)–(4), and thereby accounts for diffusion within the crystals in the model.

An asymptotic solution for the Mn^{4+} concentration has been obtained by Farrell and Please [1], and is based on two assumptions. The first is that α_1 is small. The dimensionless constant α_1 represents the ratio of the time it takes a proton to diffuse a distance y_o to the time required to discharge completely the cathode. The assumption that $\alpha_1 \rightarrow 0$ seems appropriate for all but high discharge rates (see Table 2). The second assumption is that the transfer current, $\hat{i}_n$, does not change on the timescale of crystal scale diffusion. This particular assumption is suited to particle discharge, because the reaction distribution within a single particle varies less when the particle is discharged under galvanostatic conditions. In contrast to this, within a cathode being discharged galvanostatically, each particle discharges with a varying current, and thus the transfer current is likely to vary on the timescale of crystal scale diffusion. We note that for the simplified case of constant transfer current, Eq. (27) reduces to that given by Farrell and Please.

Having obtained an expression for the concentration of Mn^{4+} ions in EMD crystals, we now turn our attention to the particle scale. The dimensionless constant α_5 represents the ratio of the time it takes electrolyte to diffuse a distance r_o to the time required to discharge completely the cathode. For all but very large particles under very high discharge rates, α_5 is small (see Table 2) and we assume that $\alpha_5 \rightarrow 0$. In addition, it is noted that the constants α_6 and α_7 are O(1) (see Table 2). Utilizing these observations in a regular perturbation analysis of Eq. (9), it is found that to leading order, the spatial variation of the electrolyte concentration on the particle scale can be eliminated from the model (see Appendix B), that is,

$$\hat{C}_{e(p)}\left(\hat{R}, \hat{r}, \hat{t}\right) = \hat{C}_e\left(\hat{R}, \hat{t}\right). \tag{29}$$

Since all spatial variation of electrolyte on the particle scale is eliminated, Eq. (10) becomes:

$$\frac{\partial \hat{\eta}_{(p)}}{\partial \hat{r}} = \hat{i}_{e(p)}\left(\left(\hat{C}_{Mn^{4+}}\big|_{\hat{y}=0.8}\right)^{-k_3} + \frac{\alpha_8}{\hat{\kappa}_{e\infty}}\right). \tag{30}$$

Combining Eq. (30) with the overpotential boundary condition given by Eq. (15), we find that at $\hat{r} = 0$:

$$\hat{i}_{e(p)} = 0. \tag{31}$$

It now becomes evident from the similarity of Eqs. (7) and (8), and Eqs. (14) and (31), that:

$$\hat{i}_{e(p)} = \hat{v}_{(p)}^{\square} \tag{32}$$

Noting this, Eqs. (17) and (18) now have the same source term and they have identical boundary conditions at $\hat{R} = 1$. Thus,

$$\hat{i}_e = \hat{v}^{\square}. \tag{33}$$

A further consequence of the loss of spatial variation within the electrolyte solution of the porous particles, as given by Eq. (29), is that the source term within Eq. (19) vanishes. This term does, however, provide a vital link within the model, between the reaction rate on the particle scale and the reaction rate on the cathode scale. Thus, rather than applying the leading order (i.e., O(α_5^0)) expansion for $\hat{C}_{e(p)}$ given by Eq. (29), in this instance a version of Eq. (9) is obtained that is accurate to O(α_5) (refer to Eq. (63) in Appendix B). Manipulation of this equation yields an expression for the source term in Eq. (19) that preserves the link between the particle and the cathode scales (refer to Eq. (66) in Appendix B). Substituting into Eq. (19) gives:

$$(1 + \alpha_{11})\frac{\partial \hat{C}_e}{\partial \hat{t}} = \frac{\alpha_{16}^2}{\alpha_5(\alpha_{17} + \hat{R})}\frac{\partial}{\partial \hat{R}}\left(\hat{D}_{e\infty}(\alpha_{17} + \hat{R})\frac{\partial \hat{C}_e}{\partial \hat{R}}\right)$$
$$- \frac{\alpha_7\alpha_{11}}{(\alpha_{17} + \hat{R})}\frac{\partial}{\partial \hat{R}}((\alpha_{17} + \hat{R})\hat{i}_e\hat{C}_e) - 3\alpha_6\alpha_{11}\hat{i}_{e(p)}\big|_{\hat{r}=1}. \tag{34}$$

On the cathodic scale, the constant α_{13} represents the ratio of the conductivity of the KOH electrolyte to the conductivity of the graphite phase. The data in Table 2 show that α_{13} is extremely small, and thus in the asymptotic limit, $\alpha_{13} \rightarrow 0$, Eq. (20) can be simplified to yield:

$$\frac{\partial \hat{\eta}}{\partial \hat{R}} = \frac{\alpha_{12}}{\alpha_{16}^2\hat{\kappa}_{e\infty}}\hat{i}_e + \alpha_9\left(1 + \frac{\alpha_{10}\hat{C}_e}{1 - \alpha_4\hat{C}_e}\right)\frac{\partial \ln \hat{a}_e}{\partial \hat{C}_e}\frac{\partial \hat{C}_e}{\partial \hat{R}}. \tag{35}$$

Eqs. (5), (7), (17), (27), (30), (34) and (35) with boundary conditions (12), (15), (21)–(23) and (25) and initial conditions (6) and (26) represent a *simplified model* of cathodic discharge for a primary alkaline battery system.

4. Solution of simplified equations

The simplified model equations are solved numerically by applying a finite-volume method [20] in which they are discretised over the radial variable on either the cathode or particle scale and in time. The reaction terms are fully linearised, and all other non-linearities are dealt with by applying a fixed-point iteration method (see, for example, [21]). The time discretisation can be adjusted by use of a weighting parameter from fully explicit to fully implicit. The solution is implemented in an extensive program using MATLAB®. The numerical algorithm used to solve the equation system steps through time and iteratively refines the solution of the discretised system of equations at each time step. If the iteration process of the solution does not converge, a smaller time step is chosen until it does. The adaptive nature of the time stepping makes the method robust over a wide parameter range. The algorithm terminates if the required cell voltage or finishing time is reached or if the time step is reduced too much.

The simplifications carried out in the previous section provide a substantial reduction in complexity of the model system, which now has only one partial differential equation, as compared with three in the full model system. The ensuing reduction in the number of numerical calculations needed to solve the system means that the software that implements the numerical solution is easily run on a standard desktop PC. For example, on a desktop machine with a 2.4 GHz Pentium® 4 processor and 512 MB of RAM, a typical discharge simulation takes of the order of 60.

4.1. Physical parameters

A list of the parameter values used in the model analysis that follows is given in Table 3. Many of the values are consistent with those given by Farrell et al. [15], but the values k_1, k_2 and k_3 were obtained by fitting the model to the experimental data of Williams [22], as discussed in Section 5.

The constant $k_1(V)$ is the coefficient of the so-called ion–ion interaction term adopted by Farrell et al. [15] in the full model. In dimensioned form, this term is given by:

$$\Upsilon = k_1(1 - C_{Mn^{4+}}\big|_{\hat{y}=1}\bar{V}_{Mn^{3+}}). \qquad (36)$$

Υ appears in dimensionless form in Eq. (5) of our simplified model. Such terms have been used by several authors [23–26] in order to overcome the fact that manganese oxide reduction is not really a single-step process, as defined by reaction (1), but rather a combination of several individual reduction processes [26–29] for which appropriate kinetic data are as yet unknown.

The constants k_2 (S cm^{-1}) and k_3 are, respectively, the pre-exponential and exponential coefficients in the manganese oxide conductivity function of the full model. In dimensioned

form, this function is given by:

$$\sigma_{EMD} = k_2\left(1 - \varepsilon_{s(p)}\right)\left(\frac{C_{Mn^{4+}}}{C_{Mn^{4+}}^0}\right)^{k_3}, \qquad (37)$$

and appears in dimensionless form in Eq. (30) of our simplified model.

5. Results and discussion

Williams [22] galvanostatically discharged a series of planar EMD cathodes in KOH electrolyte at a rate of 20, 50 or 100 mA g^{-1} of EMD. Each cathode consisted of EMD particles that were taken from a specific size fraction, namely: $2r_o \leq 45\,\mu m$, $77\,\mu m \leq 2r_o \leq 106\,\mu m$, $150\,\mu m \leq 2r_o \leq 300\,\mu m$ and $300\,\mu m \leq 2r_o \leq 500\,\mu m$. A comparison of the output of the simplified model with the experimental data of Williams is given in Fig. 2, and Table 4 lists the parameter values used in the model to simulate the experimental data.

In order to simulate the planar geometry of the experimental cathodes using the cylindrical model, the inner and outer radii of each cathode in the model are artificially increased whilst still maintaining the experimentally observed cathode thickness and cathode volume. This procedure causes the curvature of the electrode to decrease and the model equations developed in the previous section for cylindrical geometry converge to the corresponding equations for linear geometry.

From the data Fig. 2, it is seen that the model results compare well with the experimental data. The simplified model accurately captures the polarisation effects seen in the experimental results with the cathodic discharge time increasing as the EMD particle size is decreased. This is due to more uniform reaction distributions within the smaller
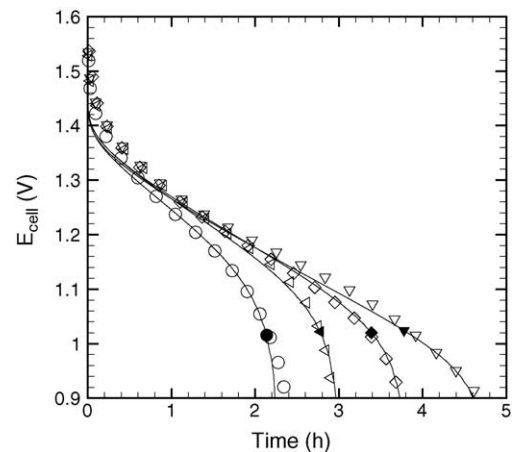

Fig. 2. Comparison between experimental discharge results (unshaded symbols) and simplified model results (shaded symbols) for planar cathodes with configuration given in Table 4. (○) r_o = 150–250 μm, (●) r_o = 180 μm, (◁) r_o = 75–150 μm, (◀) r_o = 100 μm, (◇) r_o = 38.5–53 μm, (◆) r_o = 45 μm, (▽) r_o = 0–22.5 μm and (▼) r_o = 10 μm.

EMD particles that lead to a greater utilisation of active material within cathodes containing these particles.

In simulating the data of Williams, we have taken the value of $C_{Mn^{4+}}$ that appears in the manganese oxide conductivity function (given by Eq. (37)) to be that at 80% of the radius (i.e., $0.8y_o$) of a given crystal. This corresponds to the value of $\hat{C}_{Mn^{4+}}$ at $\hat{y} = 0.8$ appearing in Eqs. (10) and (30). The effect of choosing various positions within the oxide crystals at which to take the value of $C_{Mn^{4+}}$ in order to calculate the manganese oxide conductivity is shown in Fig. 3. The simulations are for the cathode manufactured by Williams that consists of EMD particles in the size fraction $150\,\mu m \leq 2r_o \leq 300\,\mu m$ (refer to Table 4). The experimental discharge result is also given in Fig. 3.

The results in Fig. 3 indicate that taking the value of $C_{Mn^{4+}}$ at $0.8y_o$ yields a theoretical discharge that corresponds well with the experimental result. Farrell et al. [15] and Farrell and Please [1] previously took the concentration value appearing in the conductivity function to be that at the outer radius of the manganese oxide crystals. As Fig. 3 demonstrates, however, this approach appears to overestimate the resistance experienced by electrons moving within the oxide used by Williams and leads to reduced discharge times in comparison with the experimental data. To obtain more accurate predictions of the conductivity of non-uniformly reduced EMD, an in-depth study into the current paths and the connectivity on a crystal scale would be needed.

In Section 4, an expression was obtained for the concentration distribution of Mn^{4+} within an EMD crystal (i.e., Eq. (27)) by applying the method of Laplace transforms. This expression does not depend on simplifying assumptions, such as $\alpha_1 \to 0$, and that $\hat{i}_n$ does not change on the timescale of proton diffusion. Nevertheless, if we are willing to admit these two assumptions, then asymptotic methods can be applied to the crystal-scale proton diffusion problem (i.e., Eqs. (2)–(4)

and (6)) in order to obtain approximate expressions for the distribution of Mn^{4+} within EMD crystals. The analysis follows closely that reported by Farrell and Please [1] for the discharge of porous EMD particles, and we find that the O(1) expression is given by:

$$\hat{C}_{Mn^{4+}}\left(\hat{y}, \hat{r}, \hat{t}\right) = \hat{C}_{Mn^{4+}}\left(\hat{r}, \hat{t}\right) = 1 + 3\int_0^{\hat{t}} \hat{i}_n\left(\hat{r}, \hat{t}\right)\,dt^*,$$
(38)

and the O(α_1) expression is given by:

$$\hat{C}_{Mn^{4+}} = 1 + 3\int_0^{\hat{t}} \hat{i}_n\,dt^* + \alpha_1\left[\frac{\hat{y}^2}{2} - \frac{3}{10}\right]\hat{i}_n$$
$$- \alpha_1\frac{2\hat{i}_n^0}{\hat{y}}\sum_{n=1}^{\infty}\frac{\sin\left(\lambda_n\hat{y}\right)}{\lambda_n^2\sin\left(\lambda_n\right)}\exp\left(\frac{-\lambda_n^2\hat{t}}{\alpha_1}\right).$$
(39)

The discharge results (given in terms of the fraction of the theoretical capacity of the cathode that is used) of the simplified cathode model at various discharge rates are presented in Fig. 4. Either Eq. (27) or (38) is used to model the distribution of Mn^{4+} within EMD crystals. The cathode configuration used here is for a cylindrical AA-cell, details of which are given in Table 5. At low discharge rates, the use of either Eq. (27) or Eq. (38) within the model yields very similar discharge curves, however, as the current is increased, significant discrepancies between the two models are observed. To understand why these discrepancies occur, we distributions of Mn^{4+} within an EMD crystal were obtained at $R = R_i$ and $r = r_o$ as given by Eqs. (27), (38) and (39) for a discharge rates of $20\,mA\,g^{-1}$ of EMD (Fig. 5a), $50\,mA\,g^{-1}$ of EMD (Fig. 5b), or $100\,mA\,g^{-1}$ of EMD (Fig. 5c). At a low discharge rate, such as that shown in Fig. 5a, the distribution of Mn^{4+} within an EMD crystal is essentially independent of crystal radius and the simplifying assumptions that constitute the asymptotic solutions, namely, $\alpha_1 \to 0$ and that $\hat{i}_n$ does
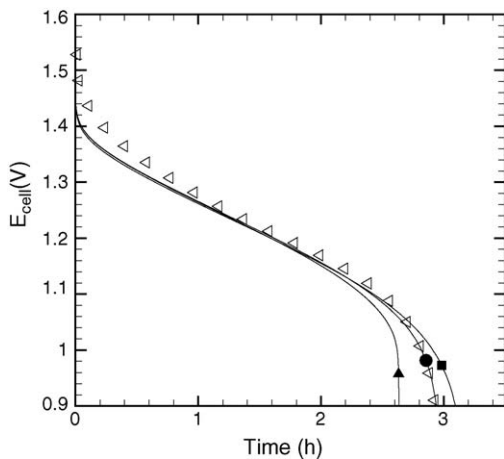

Fig. 3. Comparison between experimental discharge results (unshaded symbols) and simplified model results (shaded symbols) for a planar cathode with configuration given in Table 4 and $r_o = 75$–$150\,\mu m$ when various positions within the oxide crystals are chosen at which to calculate the manganese oxide conductivity. Conductivity calculated at (▲) y_o, (●) $0.8y_o$ and (■) $0.6y_o$.
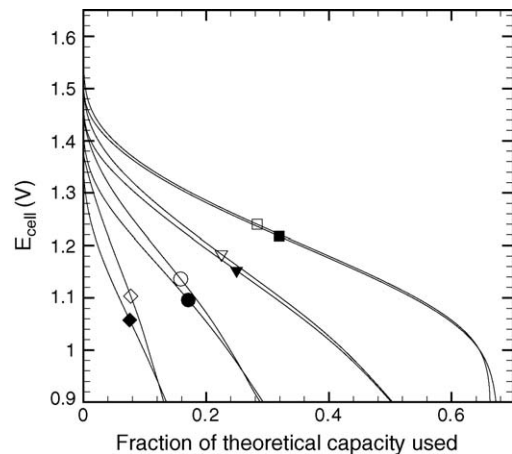

Fig. 4. Discharge results for cylindrical AA-cell as given by simplified cathode model when either Eq. (27) (unshaded symbols) or Eq. (38) (shaded symbols) is used to model the distribution of Mn^{4+} within EMD crystals. (□/■) $20\,mA\,g^{-1}$, (▽/▼) $50\,mA\,g^{-1}$, (○/●) $100\,mA\,g^{-1}$ and (◇/◆) $200\,mA\,g^{-1}$ of EMD.
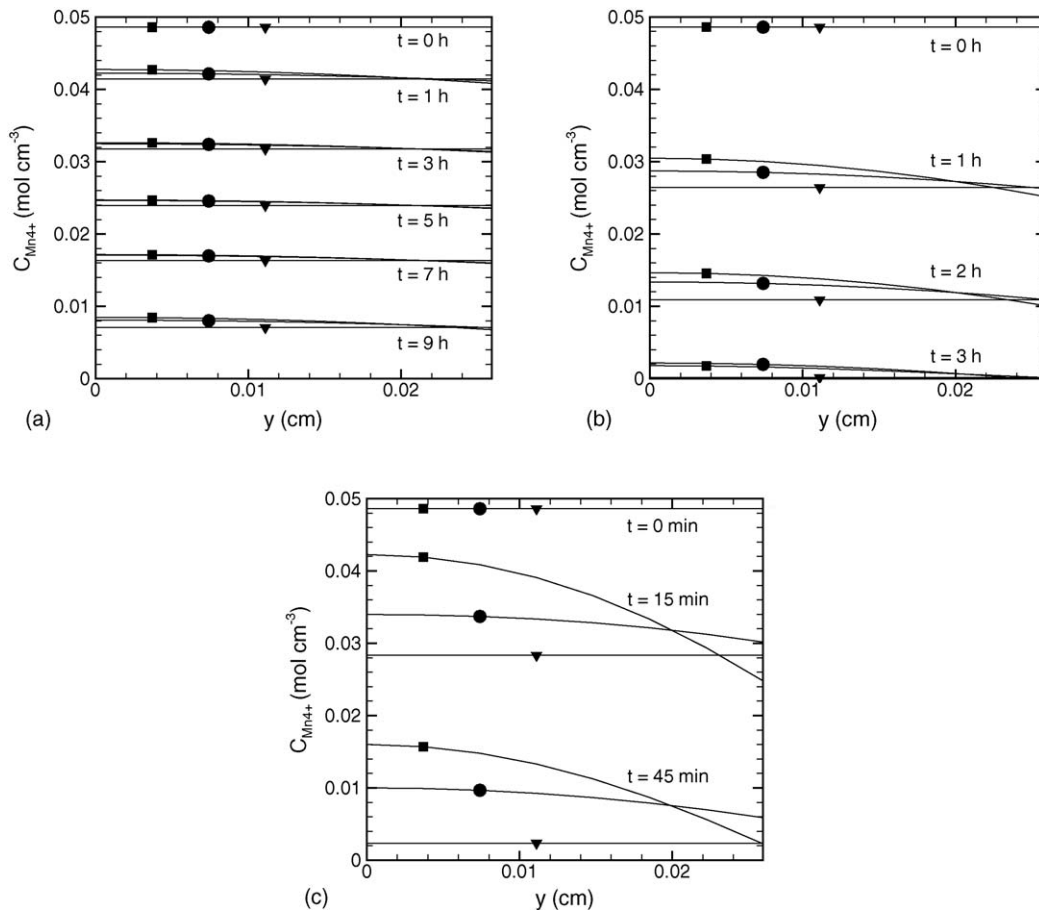
Fig. 5. Mn^{4+} concentration distributions of a crystal at $R = R_i$, and $r = r_o$ as given by Eqs. (27) (■), (38) (▼) and (39) (●) for discharge rates of (a) $20\,mA\,g^{-1}$, (b) $50\,mA\,g^{-1}$ and (c) $100\,mA\,g^{-1}$ of EMD.

not change on the timescale of proton diffusion, are well supported (in fact the α_1 value corresponding to Fig. 5a is 0.17). Thus, the results predicted by Eqs. (27), (38) and (39) correspond well in this discharge regime. When the discharge rate is increased, as in Fig. 5b and c, the distribution of Mn^{4+} within an EMD crystal becomes quite non-uniform and the discrepancies between the predictions of Eq. (27), (38) and (39) become significant. Indeed, at a discharge rate of $100\,mA\,g^{-1}$ of EMD, the assumption that $\alpha_1 \to 0$ can no longer be supported and the α_1 value corresponding to Fig. 5c is 0.86. In this regime, Eqs. (38) and (39) become invalid.

6. Conclusions

A simplified model for the galvanostatic discharge of primary alkaline battery cathodes has been presented. The simplified model was obtained by applying Laplace transform and perturbation methods to the discharge model of Farrell et al. [15]. In the analysis that ensued, it is shown that the three size scales used by Farrell et al. to describe the porous EMD cathode can be reduced to two size scales without the loss of generality. In addition, the analysis demonstrates that the time taken for electrolyte to diffuse into a porous EMD particle is fast compared with the cathodic discharge time, and that ohmic losses within the graphite phase of the cathode can be considered to be negligible. Furthermore, the simplified model incorporates a closed form expression for the distribution of Mn^{4+} within an EMD crystal that is not reliant on assumptions that may break down at high discharge rates. Numerical solutions of the simplified model equations are achieved via the use of a finite-volume code written in MATLAB® that can easily be run on a standard desktop PC. The results of the code compare favourably with relevant experimental data.

Table 5
Model input data for simulation of AA-cell set-up

Parameter	Value
Discharge rate ($mA\,g^{-1}$ of EMD)	20, 50, 100 and 200
Particle radius, r_o (cm)	100×10^{-4}
Inner radius, R_i (cm)	0.45
Outer radius, R_o (cm)	0.67
Height, H (cm)	4.04
Total mass of cathode (g)	10.62
Mass of EMD in cathode (g)	9.24
Mass of graphite in cathode (g)	0.8

Acknowledgement

Appendix A

Here, we consider the Laplace transform solution [19] of Eq. (2) subject to the boundary conditions (3) and (4) and the initial condition (6). Taking the Laplace transform of Eqs. (2) to (4), treating $\hat{i}_n$ as a function independent of $C_{Mn^{2+}}$ and substituting the initial condition (6), we obtain:

$$\frac{1}{\alpha_1}\frac{1}{\hat{y}^2}\frac{\partial}{\partial\hat{y}}\left(\hat{y}^2\frac{\partial L\left\{\hat{C}_{Mn^{4+}}\right\}}{\partial\hat{y}}\right) = pL\left\{\hat{C}_{Mn^{4+}}\right\} - 1, \qquad (40)$$

at $\hat{y} = 0$,

$$\frac{\partial L\left\{\hat{C}_{Mn^{4+}}\right\}}{\partial\hat{y}} = 0 \qquad (41)$$

and at $\hat{y} = 1$,

$$\frac{\partial L\left\{\hat{C}_{Mn^{4+}}\right\}}{\partial\hat{y}} = \alpha_1 L\left\{\hat{i}_n\right\} \qquad (42)$$

where p is the transformation variable and $L\{\gamma\}$ is the Laplace transform of γ. Using the transformation:

$$L\left\{\hat{C}_{Mn^{4+}}\right\} = \frac{1}{p} + \frac{f(\hat{y}, p)}{\hat{y}}, \qquad (43)$$

we obtain the following equation set:

$$\frac{\partial^2 f(\hat{y}, p)}{\partial\hat{y}^2} = \alpha_1 p f(\hat{y}, p), \qquad (44)$$

$$f(0, p) = 0, \qquad (45)$$

$$\frac{\partial f(1, p)}{\partial\hat{y}} - f(1, p) = \alpha_1 L\left\{\hat{i}_n\right\}. \qquad (46)$$

Solving Eq. (44) subject to the conditions (45) and (46) and substituting the result into Eq. (43), gives:

$$L\left\{\hat{C}_{Mn^{4+}}\right\} = \frac{1}{p} + \frac{\alpha_1 L\left\{\hat{i}_n\right\}\sinh\left(\sqrt{\alpha_1 p}\hat{y}\right)}{\hat{y}\left(\sqrt{\alpha_1 p}\cosh\left(\sqrt{\alpha_1 p}\right) - \sinh\left(\sqrt{\alpha_1 p}\right)\right)}. \qquad (47)$$

Applying the Convolution Theorem of Laplace transforms to Eq. (47) yields:

$$\hat{C}_{Mn^{4+}} = 1 + \int_0^{\hat{t}} \hat{i}_n\big|_{\hat{t}=\hat{t}-t^*} L^{-1}\left\{\tilde{g}(p)\right\} dt^*. \qquad (48)$$

Here, t^* is a dummy variable of integration, $L^{-1}\left\{\tilde{g}(p)\right\}$ is the inverse Laplace transform of function $\tilde{g}(p)$, where the

function $\tilde{g}(p)$ is given by:

$$\tilde{g}(p) = \frac{\alpha_1\sinh\left(\sqrt{\alpha_1 p}\hat{y}\right)}{\hat{y}\left\{\sqrt{\alpha_1 p}\cosh\left(\sqrt{\alpha_1 p}\right) - \sinh\left(\sqrt{\alpha_1 p}\right)\right\}}. \qquad (49)$$

To obtain the inverse Laplace transform in Eq. (48), an extension of Cauchy's integral formula [19] is used to write the inverse transform as an integral in the complex plane along the line $Re(z) = \gamma$, where z is the complex variable. This is the so-called complex inversion integral of $\tilde{g}(p)$, namely:

$$L^{-1}\left\{\tilde{g}(p)\right\} = \frac{1}{2\pi i}\lim_{\beta\to\infty}\int_{\gamma-i\beta}^{\gamma+i\beta}\exp\left(p\hat{t}\right)\tilde{g}(p)\,dp. \qquad (50)$$

Applying the Residue Theorem [19], the right-hand side of Eq. (50) may be written as the sum of the residues of the integrand, $\exp\left(p\hat{t}\right)\tilde{g}(p)$, at its singularities, which occur at p_m ($m = 0, 1, 2, \ldots, \infty$). It is noted that $p_0 = 0$ and $p_m = -\lambda_m^2/\alpha_1$ ($m = 1, 2, \ldots, \infty$), where the values of λ_m are given by the positive roots of Eq. (28). The first residue is 3 and the other residues are given by:

$$\frac{2}{\hat{y}}\frac{\sin\left(\lambda_m\hat{y}\right)}{\sin\left(\lambda_m\right)}\exp\left(\frac{-\lambda_m^2\hat{t}}{\alpha_1}\right); \quad (m = 1, 2, \ldots, \infty). \qquad (51)$$

Using these residues in Eq. (48), we obtain an expression for the concentration of Mn^{4+} within an EMD crystal, namely:

$$\hat{C}_4\left(\hat{y}, \hat{t}\right) = 1 + 3\int_0^{\hat{t}}\hat{i}_n\,dt^* + \frac{2}{\hat{y}}\sum_{m=1}^{\infty}\frac{\sin\left(\lambda_m\hat{y}\right)}{\sin\left(\lambda_m\right)}$$

$$\times \int_0^{\hat{t}}\hat{i}_n\big|_{\hat{t}=\hat{t}-t^*}\exp\left(\frac{-\lambda_m^2 t^*}{\alpha_1}\right)dt^*. \qquad (52)$$

Appendix B

Here, we consider the perturbation analysis of Eq. (9) subject to the boundary conditions (11) and (13) and initial condition (16), in the limit when $\alpha_5 \to 0$. We begin by expressing $\hat{C}_{e(p)}$ as an asymptotic expansion in powers of α_5, namely:

$$\hat{C}_{e(p)} \sim \hat{C}_{e,0} + \alpha_5\hat{C}_{e,1} + \alpha_5^2\hat{C}_{e,2} + \cdots \qquad (53)$$

where $\hat{C}_{e,0}, \hat{C}_{e,1}, \hat{C}_{e,2}, \ldots$ are independent of α_5. Upon substituting this expansion into Eq. (9), the following set of order equations is obtained:

$$O(\alpha_5^0): \quad \frac{1}{\hat{r}^2}\frac{\partial}{\partial\hat{r}}\left(\hat{D}_{e\infty}\hat{r}^2\frac{\partial\hat{C}_{e,0}}{\partial\hat{r}}\right) = 0. \qquad (54)$$

At $\hat{r} = 1$, $\quad \hat{C}_{e,0} = \hat{C}_e. \qquad (55)$

At $\hat{r} = 0$, $\quad \dfrac{\partial\hat{C}_{e,0}}{\partial\hat{r}} = 0. \qquad (56)$

At $\hat{t} = 0$, $\quad \hat{C}_{e,0} = 1. \qquad (57)$

$$\text{O}(\alpha_5): \quad \frac{\partial \hat{C}_{e,0}}{\partial \hat{t}} = \frac{1}{\hat{r}^2} \frac{\partial}{\partial \hat{r}} \left(\hat{D}_{e\infty} \hat{r}^2 \frac{\partial \hat{C}_{e,1}}{\partial \hat{r}} \right) - 3\alpha_6 \hat{i}_n$$

$$- \frac{\alpha_7}{\hat{r}^2} \frac{\partial}{\partial \hat{r}} (\hat{r}^2 \hat{C}_{e,0} v_{(p)}^\square) \tag{58}$$

$$\text{At } \hat{r} = 1, \quad \hat{C}_{e,1} = 0. \tag{59}$$

$$\text{At } \hat{r} = 0, \quad \frac{\partial \hat{C}_{e,1}}{\partial \hat{r}} = 0. \tag{60}$$

$$\text{At } \hat{t} = 0, \quad \hat{C}_{e,1} = 0. \tag{61}$$

Solving Eq. (54) subject to the conditions (55) to (57) gives:

$$\hat{C}_{e,0}(\hat{R}, \hat{r}, \hat{t}) = \hat{C}_e(\hat{R}, \hat{t}). \tag{62}$$

Thus, to $\text{O}(\alpha_5^0)$, the electrolyte concentration within any porous EMD particle is equal to the electrolyte concentration at the outer radius of the particle as given by $\hat{C}_e(\hat{R}, \hat{t})$.

Substituting Eq. (7) into Eq. (58), multiplying by $\hat{r}^2$ and rearranging, yields:

$$\frac{\partial}{\partial \hat{r}} \left(\hat{D}_{e\infty} \hat{r}^2 \frac{\partial \hat{C}_{e(p)}}{\partial \hat{r}} \right) - \alpha_5 \alpha_7 \frac{\partial}{\partial \hat{r}} (\hat{r}^2 \hat{C}_{e(p)} \hat{v}_{(p)}^\square)$$

$$= \alpha_5 \hat{r}^2 \frac{\partial \hat{C}_{e(p)}}{\partial \hat{t}} + \alpha_5 \alpha_6 \frac{\partial}{\partial \hat{r}} (\hat{r}^2 \hat{i}_{e(p)}). \tag{63}$$

Integrating Eq. (63) with respect to $\hat{r}$, evaluating the result at $\hat{r} = 1$ and multiplying by α_5, gives:

$$\alpha_5 \left(\hat{D}_{e\infty} \frac{\partial \hat{C}_{e,1}}{\partial \hat{r}} - \alpha_7 \hat{C}_{e,0} \hat{v}_{(p)}^\square \right) \Bigg|_{\hat{r}=1}$$

$$= \alpha_5 \left(\frac{1}{3} \frac{\partial \hat{C}_{e,0}}{\partial \hat{t}} + \alpha_6 \hat{i}_{e(p)} |_{\hat{r}=1} \right) \tag{64}$$

Noting, from Eq. (53) that

$$\alpha_5 \frac{\partial C_{e,1}}{\partial \hat{r}} = \frac{\partial C_{e(p)}}{\partial \hat{r}} + \text{O}(\alpha_5^2), \tag{65}$$

It is seen that the left-hand-side of Eq. (64) is equivalent to the source term in Eq. (19). Thus,

$$\left(\hat{D}_{e\infty} \frac{\partial \hat{C}_{e(p)}}{\partial \hat{r}} - \alpha_5 \alpha_7 \hat{C}_{e(p)} \hat{v}_{(p)}^\square \right) \Bigg|_{\hat{r}=1}$$

$$= \alpha_5 \left(\frac{1}{3} \frac{\partial \hat{C}_{e(p)}}{\partial \hat{t}} + \alpha_6 \hat{i}_{e(p)} |_{\hat{r}=1} \right). \tag{66}$$

References

[1] T.W. Farrell, C.P. Please, J. Electrochem. Soc., MS no. JES-04-0748, 2005, in press.
[2] J.S. Newman, C.W. Tobias, J. Electrochem. Soc. 109 (1962) 1183–1191.
[3] J.S. Newman, Advances in Electrochemistry and Electrochemical Engineering, Wiley, New York, 1967, pp. 87–135.
[4] J.S. Newman, T.W. Chapman, AIChE J. 19 (1973) 343–348.
[5] J.S. Newman, W. Tiedemann, AIChE J. 21 (1975) 25–41.
[6] J.S. Newman, R. Pollard, J. Electrochem. Soc. 126 (1979) 1713–1717.
[7] J.S. Newman, AIChE Symposium Series 179, 1983, pp. 55–59.
[8] J.S. Newman, Electrochemical Systems, second ed., Prentice Hall, Englewood Cliffs, NJ, 1991.
[9] W.J. Wruck, Ph.D. Thesis, The University of Wisconsin, Madison, WI, 1984.
[10] J.-S. Chen, H.Y. Cheh, J. Electrochem. Soc. 140 (1993) 1205–1213.
[11] J.-S. Chen, H.Y. Cheh, J. Electrochem. Soc. 140 (1993) 1213–1218.
[12] E.J. Podlaha, H.Y. Cheh, J. Electrochem. Soc. 141 (1994) 28–35.
[13] E.J. Podlaha, H.Y. Cheh, J. Electrochem. Soc. 141 (1994) 15–27.
[14] Y. Zhang, H.Y. Cheh, J. Electrochem. Soc. 146 (1999) 850–856.
[15] T.W. Farrell, C.P. Please, D.L.S. McElwain, D.A.J. Swinkels, J. Electrochem. Soc. 147 (2000) 4034–4044.
[16] J.J. Kriegsmann, H.Y. Cheh, J. Power Sources 85 (2000) 190–202.
[17] Y. Zhang, H.Y. Cheh, J. Electrochem. Soc. 146 (1999) 3566–3570.
[18] Delta, Private Communication with Delta EMD Australia Pty. Limited, 2003.
[19] D.W. Trim, Applied Partial Differential Equations, PWS-KENT Publishing Company, Boston, 1990, pp. 351–394.
[20] S.V. Patankar, Numerical Heat Transfer and Fluid Flow, Hemisphere Publishing Corporation, New York, 1980, p. 197.
[21] R.L. Burden, J.D. Faires, Numerical Analysis, vol. 7, Brooks/Cole, Pacific Grove, CA, 2001, pp. 602–608.
[22] R. Williams, Ph.D. Thesis, University of Newcastle, Newcastle, NSW, Australia, 1995.
[23] S. Atlung, T. Jacobsen, Electrochim. Acta 26 (1981) 1447–1456.
[24] W.C. Maskell, J.E.A. Shaw, F.L. Tye, J. Power Sources 8 (1982) 113–120.
[25] P. Ruetschi, J. Electrochem. Soc. 135 (1988) 2657–2669.
[26] Y. Chabre, J. Pannetier, Prog. Solid State Chem. 23 (1995) 1–130.
[27] Y.P. Chabre, J. Electrochem. Soc. 138 (1991) 329–330.
[28] S.W. Donne, R. Fredlein, G.A. Lawrance, D.A.J. Swinkels, F.L. Tye, in: 8th IBA Battery Materials Symposium, Brussels, 1994.
[29] S.W. Donne, Ph.D. Thesis, University of Newcastle, Newcastle, NSW, Australia, 1996.
[30] H. Zang, Z.H. Chen, X. Xi, J. Electrochem. Soc. 136 (1989) 2771.
[31] G.H. Aylward, T.J.V. Findlay, SI Chemical Data, 3rd ed., John Wiley and Sons, New York, 1994.
[32] S.U. Falk, A.J. Salkind, Alkaline Storage Batteries, John Wiley and Sons, New York, 1969, p. 577.
[33] W. Sunu, D. Bennion, J. Electrochem. Soc. 127 (1980) 2007–2016.